Computer Physics Communications 258 (2021) 107609

Contents lists available at ScienceDirect

Computer Physics Communications

journal homepage: www.elsevier.com/locate/cpc

An effective method to calculate atomic movements in 3D objects with tuneable stochasticity (3DO-SKMF)☆,☆☆

Bence Gajdics [a,b,c], János J. Tomán [a,*], Zoltán Erdélyi [a]

[a] Department of Solid State Physics, University of Debrecen, P.O. Box 400, H-4002 Debrecen, Hungary
[b] GPM, UMR 6634, University of Normandy, Saint-Etienne du Rouvray, France
[c] University of Debrecen, Doctoral School of Physics, Hungary

ARTICLE INFO

Article history:
Received 28 November 2019
Received in revised form 10 June 2020
Accepted 24 August 2020
Available online 9 September 2020

Keywords:
3D object stochastic kinetic modelling framework (3DO-SKMF)
Surface segregation
Nanoparticle
Nanowire
Core–shell
Gibbs–Thomson
Surface curvature

ABSTRACT

We present an effective computer simulation method, called 3D object stochastic kinetic modelling framework (3DO-SKMF), to calculate atomic movements in 3D objects including surface segregation and Gibbs–Thomson effect (surface curvature). Objects with any kind of shapes can easily be considered thanks to the flexibility and versatility of the model and code. Accordingly, the model and the computer code can be used in a wide variety of applications: nanoparticles, nanorods, nanotubes, nanopillars, etc. To increase the versatility of the model, it includes stochastic noise in a tuneable manner. This means that if the noise level is zero, the model is completely deterministic (mean-field), whereas by increasing the noise level the result gets closer and closer to that obtained by a kinetic Monte Carlo calculation. This allows us to calculate processes with activation barriers. Besides demonstrating the capabilities of the model, we also reproduce an experimental result showing decomposition of Ag–Cu nanoparticles.

Program summary

Program title: 3DO-SKMF
CPC Library link to program files: http://dx.doi.org/10.17632/776b7txmhv.1
Licensing provisions: CC BY NC 3.0
Programming language: ISO C
Nature of problem: Atomistic simulation of nano-objects with free surfaces by calculating occupation probabilities. The model includes surface segregation and Gibbs–Thomson effect (surface curvature).
Solution method: Numerical solution of a system of differential equations with taking into account the conservation of matter. The number of equations is equal to the number of lattice sites in a 3D lattice.
Additional comments including restrictions and unusual features: The model contains parameters that can be determined from macroscopic measurements, still in the background it follows an atomistic approach. Note that the provided code is written for nanospheres (hollow and solid), nanowires and nanotubes, however objects with any kind of shapes can easily be considered. Due to the flexibility of the code, with minor change of initialization, any 3D object can be simulated. The published code uses the face centred cubic lattice (fcc), its modification for other lattices is, however, straightforward.

1. Introduction

With the advance of nanotechnology, let it be in electronic, battery or catalytic applications, the importance of free surfaces is becoming more pronounced because with decreasing sizes the fraction of atoms on the surface increases. In a multi-component system surface segregation might emerge due to three main reasons: (i) different surface energies of the components, (ii) chemical interactions among the components (e.g. phase separation), (iii) different atomic volumes [1]. Modelling the effects of free surfaces on nano-sized systems is not a simple task as they are obviously affected by the discrete nature of the material so an atomistic point of view must be taken. Recently a new computer simulation model has been published to model the change of atomic distribution in infinite systems [2,3]. On its theoretical basis we developed an effective computer simulation method, the so-called 3D object stochastic kinetic modelling framework (3DO-SKMF), to calculate atomic movements in finite

☆ The review of this paper was arranged by Prof. D.P. Landau.
☆☆ This paper and its associated computer program are available via the Computer Physics Communication homepage on ScienceDirect (http://www.sciencedirect.com/science/journal/00104655).

* Corresponding author.
E-mail address: janos.toman@science.unideb.hu (J.J. Tomán).

https://doi.org/10.1016/j.cpc.2020.107609

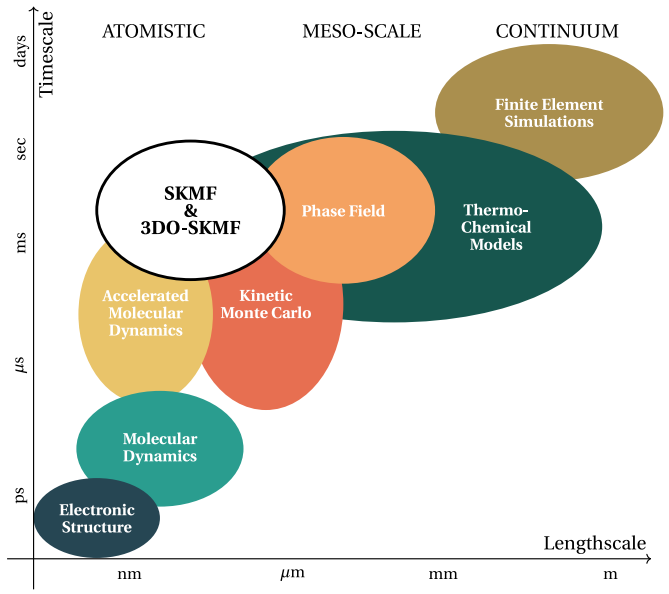

Fig. 1. Typical time and length scales of different computer simulation techniques. Figure is based on [4], but with the addition of SKMF & 3DO-SKMF.

3D objects including surface segregation and Gibbs–Thomson effect. Objects with any kind of shapes can easily be considered thanks to the flexibility and versatility of the model and code.

Accordingly, the model and the computer code can be used in a wide variety of applications: nanoparticles, hollow nanoparticles, nanorods, nanotubes etc. The typical length- and timescales that can be simulated with the method conveniently fits next to the already available techniques, as visualized on Fig. 1. To increase the versatility of the model, it includes stochastic noise in a tuneable manner. This means that if the noise level is zero, the model is completely deterministic (mean-field), whereas by increasing the noise level the result gets closer and closer to that obtained by a kinetic Monte Carlo calculation (KMC). This allows us to calculate processes with activation barriers, such as nucleation of new phases.

2. Theoretical background

First, in 1990 G. Martin proposed a 1D kinetic mean-field (KMF) model [5] then it was extended to 3D [6,7] and further developed by introducing stochastic Langevin noise [2,3] in order to examine non-deterministic processes, such as spinodal decomposition, nucleation and phase separation. The new 3DO-SKMF model can handle two-component samples with various geometric arrangements, without the requirement of using periodic boundary conditions in every directions.

A detailed reasoning can be read about the equations of this section in Ref. [8] Section 2. titled "From KMF to SKMF – Why and How". For the sake of clarity we present here the equations only with the necessary details. In the original SKMF model a fixed three-dimensional lattice is taken, on which c_i occupation probabilities are calculated (e.g. c_i gives the probability that site i is occupied by an A atom and $1-c_i$ that site i is occupied by a B atom in a binary system). The time evolution of c_i is governed by the conservation of material and the flux of occupation probability between site i and its Z nearest neighbouring sites j:

$$\frac{dc_i}{dt} = -\sum_{j=1}^{Z}\left[J_{i,j} - J_{j,i}\right]. \tag{1}$$

The J fluxes are composed of a mean-field and a stochastic part:

$$J_{i,j} = J_{i,j}^{\mathrm{MF}} + \delta J_{i,j}^{\mathrm{Lang}}, \tag{2}$$

where $J_{i,j}^{\mathrm{MF}}$ is the flux of the occupation probability of A from site i to j and of course that of B vice versa (as if material A would flow from site i to j and material B vice versa) in mean-field approximation:

$$J_{i,j}^{\mathrm{MF}} = c_i(1-c_j)\Gamma_{i,j}^{\mathrm{MF}}. \tag{3}$$

$\Gamma_{i,j}^{\mathrm{MF}}$ shows the exchange rate of the occupation probability between site i and j (similar to the exchange probability of an A atom on site i and a B atom on site j in KMC with exchange mechanism):

$$\Gamma_{i,j}^{\mathrm{MF}} = \nu \exp\left(-\frac{Q_{i,j}}{\mathrm{k}T}\right) = \nu \exp\left(-\frac{E_0 - E_{i,j}}{\mathrm{k}T}\right), \tag{4}$$

where ν is the attempt frequency, $Q_{i,j}$ is the activation energy of the exchanges, E_0 is a saddle point energy and $E_{i,j}$ is the sum of the interaction energies of sites i and j. The interaction energy of a site can be defined as a sum of the interaction energies between an atom being on the site (with a certain possibility) and atoms being (with a certain possibility) on its neighbouring sites. The interaction energy of an X (A or B) atom on site s (i or j) is therefore:

$$E_s^X = \sum_{l=1}^{Z} c_l V_{AX} + \sum_{l=1}^{Z}(1-c_l)V_{XB}, \tag{5}$$

where we assume that the first coordination shell of the given site consists of Z sites and the probability of the neighbouring l site being occupied by A or B is c_l and $1-c_l$, respectively. V_{AA}, V_{BB} and V_{AB} are the A–A, B–B and A–B pair interaction energies. We must note that though throughout this work we consider only nearest neighbour interactions, SKMF is not limited to them. One can consider further interaction shells [8] or even n-body potentials. Also, due to the continuous nature of the finding probabilities on the lattice sites, composition dependent interaction energies can also be easily implemented [9] and combination with other methods to form multi-scale techniques can be conveniently realized [10].

One can introduce $M = (V_{AA} - V_{BB})/2$ that accounts for the A/B asymmetry of the tracer diffusion coefficients. Thereby, different values for the parameter M without affecting the equilibrium state will result in different kinetic pathways towards equilibrium (e.g. interface sharpening instead of broadening in miscible alloys [11,12]). Introducing also $V = V_{AB} - (V_{AA} - V_{BB})/2$ regular solid solution parameter (that is proportional to the heat of mixing) and $\Gamma_0 = \exp\{-E_0/\mathrm{k}T\}$, a different formalism can be used for $\Gamma_{i,j}^{\mathrm{MF}}$:

$$\Gamma_{i,j}^{\mathrm{MF}} = \Gamma_0 \exp\left(\frac{E_{i,j}}{\mathrm{k}T}\right), \tag{6}$$

where

$$E_{i,j} = (M-V)\sum_{\substack{l=1,\\ l\in\mathcal{V}(i)}}^{Z} c_l + (M+V)\sum_{\substack{l=1,\\ l\in\mathcal{V}(j)}}^{Z} c_l + Z(V_{AB}+V_{BB}). \tag{7}$$

The summation spans sites in the vicinity $\mathcal{V}(i)$ of site i and in the vicinity $\mathcal{V}(j)$ of site j in the first and second term, respectively.

Along with the flux of occupation probability predicted by mean-field approximation an additional $\delta J_{i,j}^{\mathrm{Lang}}$ dynamic Langevin noise term is used:

$$\delta J_{i,j}^{\mathrm{Lang}} = c_i(1-c_j)\frac{A_n}{\sqrt{dt}}\sqrt{3}(2u-1), \tag{8}$$

where dt is the timestep of the simulation and u is a uniform random number on the [0, 1) interval. A_n noise amplitude gives

the opportunity to tune the system from fully deterministic ($A_n = 0$) solution to stochastic cases. In present work we focus on the improvements on the original model. If the reader is interested in the introduced stochasticity, hereby we refer to some of the recent publications on the topic. The nature of the resulting probability fluctuations, their correlations and the comparison to kinetic Monte Carlo simulations has been discussed in Ref. [13]. Detailed theoretical considerations are published in the Supplementary Materials of [13] and in [14]. A recent application of noise in the early stages of a multi-scale modelling of phase-separation has been published in [10].

3. New framework

The equations introduced in the previous section are true for the bulk that is periodic boundary condition has to be applied when doing computer simulation. In finite samples, however, periodic boundary condition cannot be used anymore, thus a new approach must be introduced with new equations, which modifies the numerical algorithm as well. We show a way of taking the surface effects into account in the following section.

3.1. Equations for 3D objects with free surfaces

The equations near the surface can be described based on the broken bond model (BBM) [15], in which we assume that the first coordination shell of a given i site consists of $Z - B_i$ sites, where B_i defines the number of broken bonds. Similarly to Eq. (5), the interaction energies are modified taking the broken bonds into account:

$$E_s^X = \left[\sum_{l=1}^{Z-B_s} c_l V_{AX} + \sum_{l=1}^{Z-B_s} (1 - c_l) V_{BX} \right] . \tag{9}$$

The summation runs over the first neighbouring sites, where $Z - B_s$ is the total number of atomic sites in the first coordination shell.

$\Gamma_{i,j}^{\mathrm{MF}}$ exchange rate must be written in a new form, which contains the surface effect:

$$\Gamma_{i,j}^{\mathrm{MF}} = \Gamma_0 \exp\left(\frac{E_{i,j}^S}{\mathrm{k}T}\right). \tag{10}$$

After some algebra, taking into account the BBM [16], one can find that $E_{i,j}^S$ changes to:

$$E_{i,j}^{S,BBM} = (M - V) \sum_{\substack{l=1,\\ l\in\mathcal{V}(i)}}^{Z-B_i} c_l + (M + V) \sum_{\substack{l=1,\\ l\in\mathcal{V}(j)}}^{Z-B_j} c_l + \tag{11}$$
$$+ \frac{1}{2}\left(B_j - B_i\right) V + \frac{1}{2}\left(B_j - B_i\right) M + \left(Z - \frac{B_i + B_j}{2}\right)(V_{AB} + V_{BB}) .$$

The $\frac{1}{2}\left(B_j - B_i\right) V$ term together with the first two summation terms cause surface segregation due to the chemical interaction between the components. The $\frac{1}{2}\left(B_j - B_i\right) M$ term is responsible for the surface segregation due to difference of the surface energies of the components. The last term is a composition independent term and is responsible for the different exchange rates in the bulk and close to the surface If both B_i and B_j are 0, i.e. both sites have the full set of first neighbours, Eq. (11) gives Eq. (6) bulk equation back. The appearance of $M = (V_{AA} - V_{BB})/2$ in the fourth term is concerning, as this shows, how in the simple BBM, diffusion asymmetry and surface segregation are linked to each other through the pair interaction energies. In reality, they are, however, often not linked; for example in the Ag–Cu system the diffusion asymmetry is negligible [17], but a strong surface segregation can be observed [18].

Instead of using M for tuning the surface segregation one can introduce σ^* that is the difference of the specific surface energies of A and B materials:

$$\sigma^* = -\frac{\sigma_A - \sigma_B}{n_0 B_{\mathrm{surf}}}, \tag{12}$$

where σ_A and σ_B are the surface energies of A and B while n_0 is the number of atomic sites per unit surface and B_{surf} is the number of broken bonds per atom on the surface.

Similarly, for the last term in Eq. (11), once we understood what is its role in the equation, instead of the simple pair interaction energies one can use a more phenomenological approach and introduce

$$\varepsilon^* = \frac{1}{B_{\mathrm{surf}}} \frac{\Gamma_{\mathrm{surf,surf}}}{\Gamma_{\mathrm{bulk,bulk}}}, \tag{13}$$

where $\Gamma_{\mathrm{surf,surf}}$ is the exchange rate between two sites on the surface, both with B_{surf} number of broken bonds and $\Gamma_{\mathrm{bulk,bulk}}$ is the exchange rate between two sites in the bulk, both with the full set of Z neighbours. A schematic visualization of these relationships can be seen in Fig. 2.

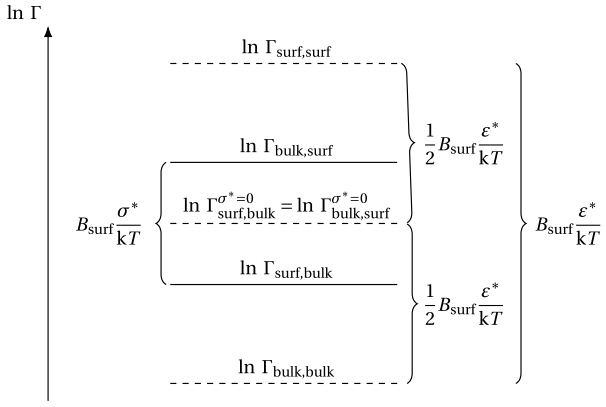

Fig. 2. Schematic figure about the role of ε^* and σ^* parameters in 3DO-SKMF simulations.

Consequently instead of the simple BBM and $E_{i,j}^{S,BBM}$ we can use:

$$E_{i,j}^S = (M - V) \sum_{\substack{l=1,\\ l\in\mathcal{V}(i)}}^{Z-B_i} c_l + (M + V) \sum_{\substack{l=1,\\ l\in\mathcal{V}(j)}}^{Z-B_j} c_n + \tag{14}$$
$$+ \frac{1}{2}\left(B_j - B_i\right) V - \frac{1}{2}\left(B_j - B_i\right) \sigma^* + \left(Z - \frac{B_i + B_j}{2}\right) \varepsilon^*,$$

where σ^* is the difference of the specific surface energies of A and B materials, while ε^* controls how fast the diffusion is close to the surface compared to the bulk material. Together with Γ_0 the last term could be viewed as a saddle point energy the value of which depends on the number of broken bonds of the sites involved in the exchange.

3.2. Simulation method

In this section we will discuss in detail the general structure of the program and solution algorithm. For the sake of clarity throughout the description we restrict ourselves to the specific case of the spherical nanoparticle. During the numerical calculations we solve the dimensionless form of the equations. The reduced quantities used are the reduced timestep $\Delta\tau = \Delta t \Gamma_0$, reduced noise amplitude $\widetilde{A}_n = A_n/\sqrt{\Gamma_0}$, reduced fluxes $\widetilde{J}_{i,j} = J_{i,j}/\Gamma_0$, furthermore M, V, σ^* and ε^* are used in kT units, for which

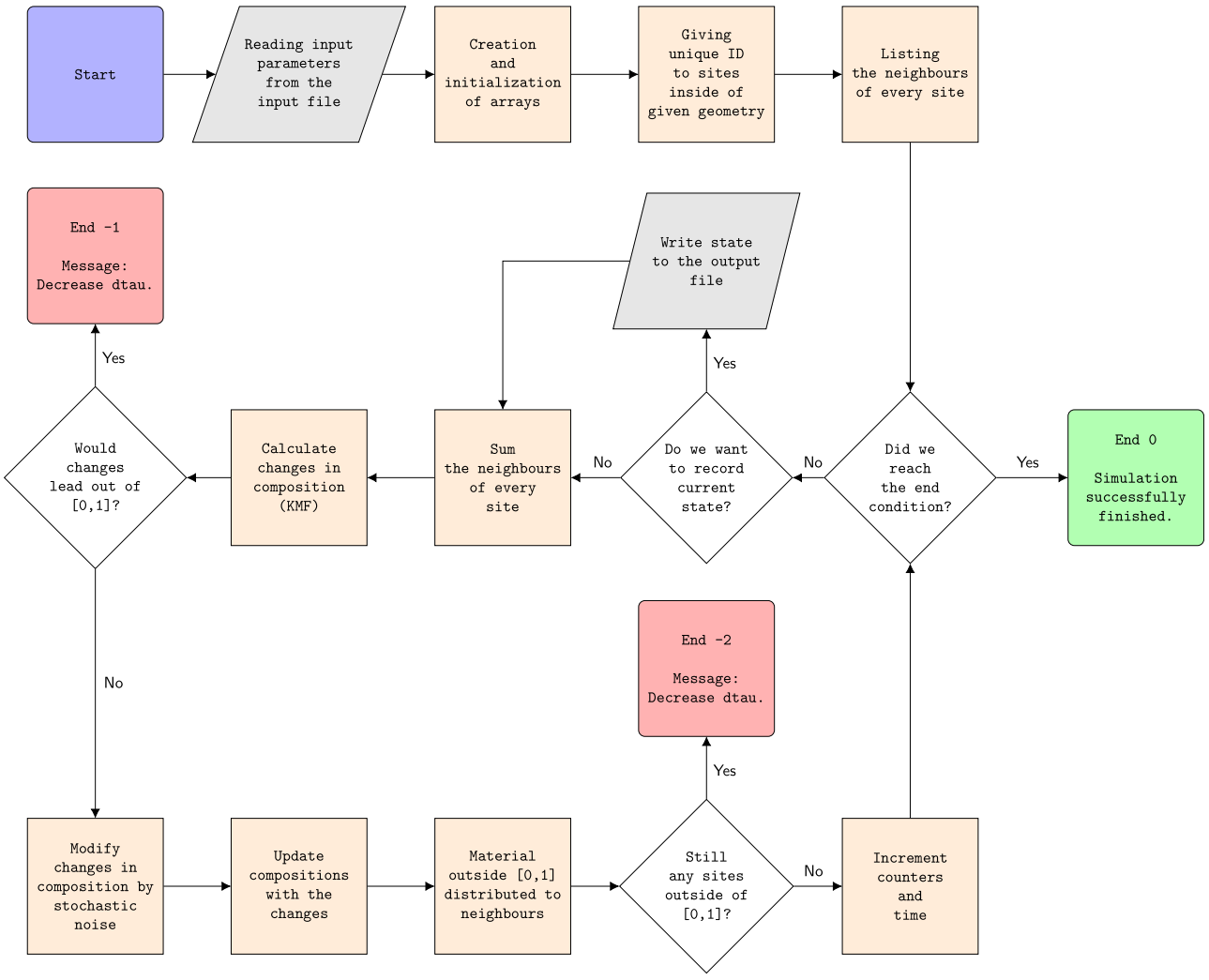

Fig. 3. Schematic flowchart diagram showing the main steps of the 3DO-SKMF method.

we use the $\widetilde{M}$, $\widetilde{V}$, $\widetilde{\sigma}^*$ and $\widetilde{\varepsilon}^*$ notation, respectively. Distances are measured in d units that is the lattice distance in (1 0 0) direction, thus the dimensionless radius is $\widetilde{R} = R/d$. The structure of the program is visualized in Fig. 3.

At the beginning of our simulations, parameters are being read from a formatted input file determining the physical properties of the system ($\widetilde{R}$, $\widetilde{M}$, $\widetilde{V}$, $\widetilde{\sigma}^*$, $\widetilde{\varepsilon}^*$ and c_0 initial composition) and the simulation parameters ($\widetilde{A}_n$, $\Delta\tau$, `Ss` number of timesteps between saving records and the totally required `Ns` number of records). In Table 1 we collected the input parameters and their equivalent variable in the program code.

The following step is the initialization of the necessary arrays. In the original SKMF method, an atomic site having `x,y,z` coordinates was interpreted as the `i,j,k` element of the three dimensional `c` composition array, thus `x,y,z` coordinates were natural numbers.

In 3DO-SKMF each site gets a unique ID from `1` to `N`, where `N` is the total number of sites. This way memory allocation is avoidable for the empty atomic sites. It is a satisfactory condition to find a possible site in the case of an fcc structure, if the sum of the absolute values of coordinates is even. Three additional `x[N],y[N],z[N]` new arrays are being used storing the coordinates of the ith element. Note that using distances normalized by (1 0 0) planar distance d and choosing the coordinate system according to the base vectors of the fcc lattice, the coordinates are still integer numbers. All of these are dynamically allocated arrays in our software. The shape of the sample must be defined through functions or conditions, but this geometry can be arbitrary. In the case of a simple nanoparticle, all the sites inside a sphere with radius `R` will be listed as an active array element, where `R` is also defined in the units of d. During initialization every new site will receive the upcoming ID number, the size of the arrays are increased and the initial composition of the site is being set to c_0, which is an input parameter as well. For the sake of optimizing the search for neighbours in the next step, the unique ID's of the sites are given in a specific order. We start with the site in the middle of the system and in every cycle we only consider sites that are within a $[R_i; R_i+d)$ distance range (layer) from the centre. This way we can store which ID's belong to a certain layer. For this we use the `layer_start[R]` array in which in its `i`th element we store the ID of the first particle starting the `i`th layer.

After the initialization step, each sites' neighbouring sites are stored in dedicated arrays. The array `numn[i]` stores the number of neighbouring sites of site i and `nn[i][j]` lists the ID's of the `j`th neighbouring sites of `i`. In the case of fcc, all the first neighbours are at a distance of $\sqrt{2}$ distance units from a given i site. The simplest way is creating a search function calculating the distance between each particle pair's coordinates and storing

Table 1
Input parameters of 3DO-SKMF.

Program variable	Sign	Description
`M_per_kT`	$\widetilde{M}$	Diffusion asymmetry parameter in kT units
`V_per_kT`	$\widetilde{V}$	Mixing energy parameter in kT units
`An_tilde`	$\widetilde{A}_n$	Noise amplitude in $\sqrt{\Gamma_0}$ units
`dtau`	$\Delta\tau$	Dimensionless timestep in $1/\Gamma_0$ units
`c_start`	c_0	Starting composition
`Eps_per_kT`	$\widetilde{\varepsilon}^*$	Surface diffusion parameter in kT units
`Sig_per_kT`	$\widetilde{\sigma}^*$	Surface segregation parameter in kT units
`r`	$\widetilde{r}$	Inner radius in d units
`R`	$\widetilde{R}$	Outer radius in d units
`L`	$\widetilde{L}$	Length of nanowire or -tube in d units. Value must be even. If set to 0, then the system is spherical.
`Ss`		Frequency of saving data in dtau units
`Ns`		Stop if number of saved states reaches this value

the matches. It is performed only once during the simulation, but this solution is very inefficient for large nanoparticles. In the published version of the code the search is optimized for checking only particle ID's which are on the same layer or within the next two layers. Note, that to avoid double checking of the same particle pairs, it is always enough to consider only particle ID's higher than the currently checked particle's ID. In the case of an fcc lattice, the maximum number of first neighbours is 12, which is the Z total coordination number. Inside the sample, all of the sites have Z first neighbours, whereas closer to the surface region of the sample, the sites do not have the full set of 12 neighbours. The difference between Z and `numn[i]` gives the number of broken bonds B_i at the selected site.

The following step is the simulation of the kinetic processes in the main calculation loop.

Data is recorded at the beginning of the cycle. Output files are created in extended *.xyz* format, readable for the visualization software OVITO [19]. Coordinates and corresponding compositions are written in the output file in regular intervals. Recording frequency and the total number of saves are input parameters and adjustable.

At each i site the sum of composition over the first neighbours are calculated, which is necessary in order to determine the activation energies based on Eq. (14)). Using that with Eq. 1–(3) and ((10) the dc_i rates of change of c_i compositions are being calculated and stored. Before updating `c` array, one must make sure that dc_i will not lead the value of c_i out from the [0, 1] composition range. If it happens so, $\Delta\tau$ time step should be decreased in the input file, because the KMF cycle is unstable.

Then the dynamic Langevin noise is being applied on the system using the formula Eq. (8), which will affect the previously defined dc_i values derived from deterministic calculation. At this point, c array is updated with the noise-affected dc. It must be noted that a high amplitude of noise and/or extreme system parameters can cause composition values out of the [0, 1] range. In order to tackle this issue, a composition redistribution method was introduced, in which the excess material is distributed between the first neighbouring sites with weights based on their actual compositions. The details of this method was already discussed in [2]. After the back-distribution cycle, the composition array is checked again. The $d\tau$ time step should be additionally decreased in case of remaining c values outside of [0, 1] range after redistribution. The main loop runs until the simulation reaches the number of recorded states defined by the input file.

4. 3DO-SKMF in use

We demonstrate the applicability of the developed technique on a few cases: (i) a completely miscible binary alloy with surface segregation in spherical nanoparticle and infinite nanotube shapes, (ii) a hemispherical nanoparticle made of a phase-separating alloy, like Ag–Cu, (iii) an ideal alloy with surface segregation forming a hollow nanosphere.

4.1. Ideally mixing alloy with surface segregation

The most simple test that can be done is a spherical nanoparticle with setting $V = 0$ and $M = 0$, which is an ideal solid solution without diffusion asymmetry, but changing the value of σ^*, which is responsible for the segregation of A or B atoms on the surface.

One can find that in this case the chemical segregation does not take place, however the effect of the surface segregation, due to the missing bonds will appear. Simulations were done using $c_0 = 0.5$ initial composition at each site in both cases. As Fig. 4 shows, core–shell structure has formed, where red and blue represent the majority A and the majority B sites, respectively. By changing the sign of $\widetilde{\sigma}^*$ from positive to negative, the segregating species can be changed.

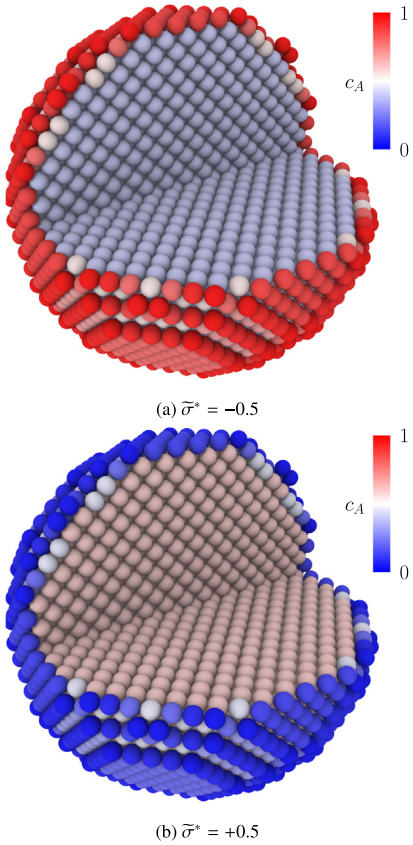

(a) $\widetilde{\sigma}^* = -0.5$

(b) $\widetilde{\sigma}^* = +0.5$

Fig. 4. Segregation of A and B on the surface of a nanosphere (one quarter removed for visualization) ($\widetilde{R} = 15, c_0 = 0.5, \widetilde{A}_n = 0, \widetilde{V} = 0.0, \widetilde{M} = 0.0$).

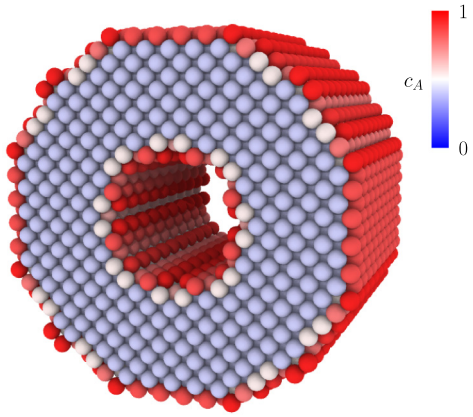

Fig. 5. Core–shell structure formation in an infinite nanotube ($\widetilde{R} = 10, c_0 = 0.5, \widetilde{A}_n = 0.0, \widetilde{V} = 0.0, \widetilde{M} = 0.0, \widetilde{\sigma}^* = -0.5$).

Nanowire and nanotube structures can also be simulated based on this method. Fig. 5 shows obtained results on the formation of a core–shell geometry in an infinite hollow nanotube, where periodic boundary condition was used in longitudinal direction, but surface segregation was allowed at the free surfaces (both inner and outer ones).

4.2. Phase-separating hemispherical nanoparticle

We have investigated spinodal decomposition in hemispherical nanoparticles and have found similar structure formation as the experimentally observed results in Ag–Cu system after codeposition [20]. Fig. 6(a) shows an Ag–Cu nanoparticle decomposed into Ag- and Cu-rich phases. Fig. 6(b) is a 3DO-SKMF simulation result, where the phase separation of *A* and *B* (representing Ag and Cu atoms) takes place as well. The simulation was started from a homogeneous state with minor dynamic noise introduced. The resulting composition profiles of the particle's cross section can be seen in Fig. 6(d).

As expected, some desegregation is observed near the surfaces due to the chemical effect. In Fig. 6(c) we show how the surface composition values are close to the ones calculated from a single-layer Fowler–Guggenheim approximation. Nevertheless, such small changes in composition cannot be detected on a microscope image.

4.3. Gibbs–thomson effect in a hollow nanosphere

The Gibbs–Thomson effect, in general, refers to variations in chemical potential (or vapour pressure) across a curved surface (interface). As a consequence, the surface composition in a multicomponent system is expected to differ in case of a curved surface from that of a flat surface — the higher the curvature, the greater the difference.[21] This phenomenological explanation needs to be translated to atomistic interpretation to understand how this effect can be considered in an atomistic model.

In an atomistic picture, in the simplest case, a curved surface differs from a flat one in the number of broken bonds (BB) — the higher the curvature, the greater the difference. Obviously, the chemical potential at the surface is related to the number of BB resulting in the Gibbs–Thomson effect. As the surface segregation effect is also related to the number and type of BB, it is expected that the curvature – Gibbs–Thomson effect – also affects the

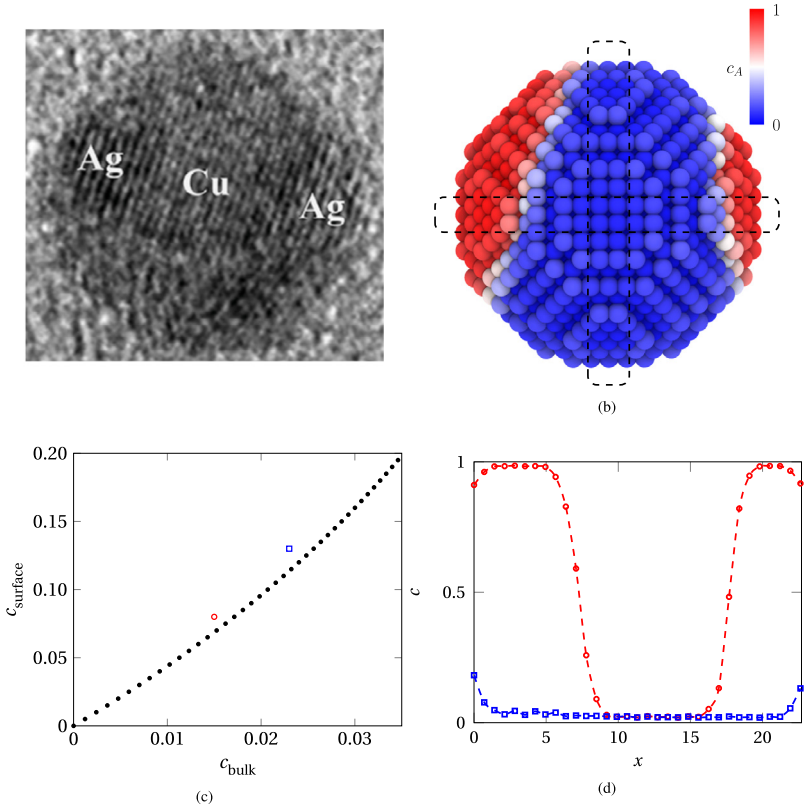

Fig. 6. Phase separation in a Ag–Cu hemispherical nanoparticle: experimental (a) [20] and simulation (b) results. The corresponding line concentration profile is shown in (d) ($\widetilde{R} = 12, c_0 = 0.3, \widetilde{A}_n = 0.05, \widetilde{V} = 0.35, \widetilde{M} = 0, \widetilde{\sigma}^* = 0$). The dashed rectangles in (b) show the areas where the line profiles were calculated from. In (c) the surface compositions plotted in two cases as a function of the bulk compositions close to the sampled surface. The dotted line shows the prediction by the single-layer Fowler–Guggenheim isotherm.

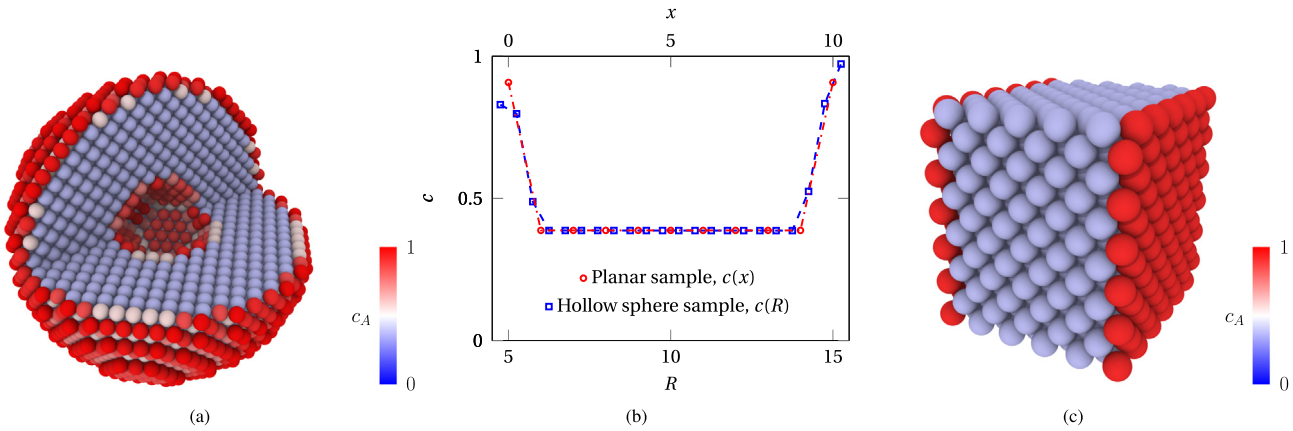

Fig. 7. Demonstration of the Gibbs-Thomson effect in surface segregation emerging due to the curvature of the surface: (a) hollow nano particle – for better visualisation, a quarter of the particle is removed ($\widetilde{R} = 15.5, \widetilde{r} = 4.5, c_0 = 0.5, \widetilde{A}_n = 0.0, \widetilde{V} = 0.0, \widetilde{M} = 0.0, \widetilde{\sigma}^* = -0.7$), (b) composition profiles deduced from (a) and (c), (c) flat membrane ($\widetilde{A}_n = 0.0, \widetilde{V} = 0.0, \widetilde{M} = 0.0, \widetilde{\sigma}^* = -0.7$, starting composition is set to result in the same bulk composition as in subfig. (a)).

surface segregation, that is the equilibrium surface composition is curvature dependent.

After having understood the atomistic picture of the Gibbs–Thomson effect, we can immediately see that the 3DO-SKMF considers this inherently. To test and demonstrate this effect, we performed equilibrium calculations for a hollow nanoparticle (Fig. 7(a)) and a flat membrane (Fig. 7(b)) with the same composition far from the surface. As can be seen either in these figures, or even better in the composition profiles deduced from these (Fig. 7(c)), the surface composition does not differ at the two surfaces of the planar sample, whereas it is markedly different at the outer surface of the hollow particle and at the inner one. Note also that the surface composition of the membrane is between that of the outer and inner surface composition of the hollow particle, which means that the concave and convex curvature influences the surface composition in the opposite way, just as expected on the basis of the phenomenological Gibbs–Thomson picture.

5. Summary

In this paper, we have shown an effective computer simulation method, called 3D object stochastic kinetic modelling framework, 3DO-SKMF, to calculate atomic movements in 3D objects including surface segregation and the Gibbs–Thomson effect. Objects with any kind of shapes can easily be considered thanks to the flexibility and versatility of the model and code. Accordingly, the model and the computer code can be used in a wide variety of applications: nanoparticles, nanorods, nanotubes, nanopillars, etc. To increase the versatility of the model, it includes stochastic noise in a tuneable manner. This allows us to calculate processes with activation barriers. To demonstrate the capabilities of 3DO-SKMF, we presented some examples – flat membrane, nanotube, hollow nanoparticle – and we also reproduced experimental results showing decomposition in Ag–Cu binary hemispherical nanoparticles.

Declaration of competing interest

The authors declare that they have no known competing financial interests or personal relationships that could have appeared to influence the work reported in this paper.

Acknowledgement

The research was financed by the Higher Education Institutional Excellence Programme (NKFIH-1150-6/2019) of the Ministry of Innovation and Technology in Hungary, within the framework of the Energetics thematic programme of the University of Debrecen.

References

[1] D. Beke, C. Cserháti, Z. Erdélyi, I. Szabó, in: H. Nalwa (Ed.), Nanoclusters and Nanocrystals - Stevenson Ranch, American Scientific Publishers, 2003, pp. 211–252.
[2] Z. Erdélyi, M. Pasichnyy, V. Bezpalchuk, J.J. Tomán, B. Gajdics, A.M. Gusak, Comput. Phys. Comm. 204 (2016) 31–37.
[3] http://skmf.eu.
[4] M. Stan, Mater. Today 12 (11) (2009) 20–28.
[5] G. Martin, Phys. Rev. B 41 (4) (1990) 2279–2283.
[6] N.V. Storozhuk, K.V. Sopiga, A.M. Gusak, Phil. Mag. 93 (16) (2013) 1999–2012.
[7] V.M. Bezpalchuk, A.M. Gusak, Metallofiz. Noveish. Tekhnol. 37 (2015) 1583–1593.
[8] A. Gusak, T. Zaporozhets, N. Storozhuk, J. Chem. Phys. 150 (17) (2019) 174109.
[9] B. Gajdics, J.J. Tomán, Z. Erdélyi, CALPHAD 67 (2019) 101665.
[10] B. Gajdics, J.J. Tomán, H. Zapolsky, Z. Erdélyi, G. Demange, J. Appl. Phys. 126 (6) (2019) 065106, http://dx.doi.org/10.1063/1.5099676.
[11] Z. Erdélyi, M. Sladecek, L.-M. Stadler, I. Zizak, G.A. Langer, M. Kis-Varga, D.L. Beke, B. Sepiol, Science 306 (5703) (2004) 1913–1915.
[12] Z. Erdélyi, I.A. Szabó, D.L. Beke, Phys. Rev. Lett. 89 (2002) 165901.
[13] T.V. Zaporozhets, A. Taranovskyy, G. Jáger, A.M. Gusak, Z. Erdélyi, J.J. Tomán, Comput. Mater. Sci. 171 (2020) 109251, http://dx.doi.org/10.1016/j.commatsci.2019.109251.
[14] A. Gusak, T. Zaporozhets, Metallofiz. Noveishie Tekhnol. 40 (11) (2018) 1415–1435, http://dx.doi.org/10.15407/mfint.40.11.1415.
[15] Z. Erdélyi, D.L. Beke, Phys. Rev. B 70 (2004) 245428.
[16] C. Cserháti, H. Bakker, D. Beke, Surf. Sci. 290 (3) (1993) 345–361.
[17] D.B. Butrymowicz, J.R. Manning, M.E. Read, J. Phys. Chem. Ref. Data 3 (2) (1974) 527–602.
[18] J.R. Chelikowsky, Surface Sci. 139 (2) (1984) L197–L203.
[19] A. Stukowski, Modelling Simulation Mater. Sci. Eng. 18 (1) (2009) 015012, http://dx.doi.org/10.1088/0965-0393/18/1/015012.
[20] G. Radnóczi, E. Bokányi, Z. Erdélyi, F. Misják, Acta Mater. 123 (2017) 82–89.
[21] M. Perez, Scr. Mater. 52 (8) (2005) 709–712.